APPENDIX:

TABLE OF CONTENT

Page 1-3: appendix figure legends.

Page 4-8: appendix figures S1-S5.

Appendix Figure S1. Mettl14 regulates skin tissue homeostasis and wound healing. (A) Immunoblots show reduced level of Mettl14 upon calcium (Ca) shift-induced differentiation of epidermal progenitor cells. Hi: High. **(B)** Representative genotyping results for mice bearing *Mettl14*^{fl} and *K14-Cre* alleles. fl: floxed. **(C)** Level of total RNA m^{6}A modification in WT and *Mettl14* cKO skin were determined by mass spectrometry and shown as box and whisker plots. The plot indicates the mean (solid diamond within the box), 25th percentile (bottom line of the box), median (middle line of the box), 75th percentile (top line of the box), 5th and 95th percentile (whiskers), 1st and 99th percentile (solid triangles) and minimum and maximum measurements (solid squares). n=9 (biological repeats), P<0.01 (Student's t-test). **(D)** The thickness of skin epidermis in WT or *Mettl14* cKO animals was quantified and shown as box plots. n=18; P<0.01 (Student's t-test). **(E)** The number of suprabasal epidermal cells in WT or *Mettl14* cKO animals was quantified and shown as box plots. n=50; P<0.01 (Student's t-test). **(F)** Representative images of skin wounds in WT and cKO animals at different time points. Scale bars represent 2.5 cm.

Appendix Figure S2. Loss of *Mettl14* impairs epidermal stemness. (A) Immunohistochemistry staining (Ki67) shows similar epidermal proliferation in WT and *Mettl14* cKO skin. **(B)** Diagram depicting the design of EdU (5-ethynyl-2'-deoxyuridine) pulse-chase experiments. **(C)** EdU incorporation assay shows reduced proliferation capability of *Mettl14* null cells *in vitro.* n=6; P<0.01 (Student's t-test). **(D)** CFE (colony formation efficiency) of WT, *Mettl14* KO, and KO cells with re-expression of *Mettl14* or *Mettl14* R298P mutant was determined *in vitro*. Error bar represents S.D.

Appendix Figure S3. Mapped enrichment results from RNA methylome profiling. Transcripts with at least two-fold decrease in m^{6}A level in differentiated vs. undifferentiated cells were

analyzed and visualized for overrepresented GO Biological Process terms using Cytoscape with Bingo plugin. Nodes represent gene sets with shared enrichment annotation. Diameter of nodes correspond to the number of genes associated with enrichment term. The color of the node represents the corrected *p* value. White nodes are not over-represented, whereas colored nodes are over-represented.

Appendix Figure S4. Pvt1 regulates epidermal stemness and tissue homeostasis. (A) Targeting strategy for deletion of *Pvt1* in cultured mouse epidermal progenitor cells. iCas9: inducible Cas9. gRNA: guide RNA. **(B)** mRNA level of *MYC* was determined by RT-PCR in WT and *Pvt1* inducible KO cells. The result shows no significant changes of *MYC* transcription upon partial loss of *Pvt1.* Data from biological replicates. All error bars represent S.D. **(C)** Decrease of *Pvt1* level upon transfection of siRNA, as determine by RT-PCR. **(D)** CFE of WT control cells and cells with *Pvt1* knockdown (siRNA). **(E)** Pairing of A282, A294, and A446 in predicted Pvt1 secondary structure. **(F)** Expression of *Pvt1* A5GT3C mutant cannot restore CFE *in vitro,* resembling the effect of A5G mutant of *Pvt1.* **(G)** The number of Krt10 (Keratin 10)-positive epidermal cells in WT or *Pvt1* inducible KO skin grafts was quantified and shown as bar graphs. n=4; P<0.01 (Student's t-test). Error bar represents S.D. (standard deviation). **(H)** The number of suprabasal epidermal cells in WT or *Pvt1* inducible KO skin grafts was quantified and shown as box plots. n=14; P<0.01 (Student's t-test).

Appendix Figure S5. Pvt1 methylation regulates epidermal stemness through its interaction with MYC. (A) Gene set enrichment analysis (GSEA) on RNA-seq data. The hallmark (H) gene sets curated from the Molecular Signatures Database (MSigDB) was analyzed for enrichment significance with 1000 random permutation of gene sets and showed that MYC-

targeted gene sets are significantly enriched (nominal-p<0.001, FDR-q<0.25) in epidermal progenitor cells. **(B)** *Pvt1* m^6A methylation level was determined by α-m^6A immunoprecipitation followed with RT-PCR. Treatment of FTO can significantly reduce Pvt1 methylation. All error bars represent S.D. **(C)** Interaction between Pvt1 or Pvt1 mutant with MYC was determined by immunoprecipitation followed with RT-PCR and quantified as bar graphs. n=8; P<0.01 (Student's t-test). Error bar represents S.D. **(D)** Immunoblots show similar amount of MYC proteins in the immunoprecipitation for determination of MYC and Pvt1 interaction (Figure 4A and Supplementary Fig. 5B). **(E)** Band intensity of MYC at different time points after cycloheximide treatment is determined by densitometry and the amount of MYC is calculated and quantified. n=3. Error bar represents S.D. **(F)** Ectopic expression of *MYC* can increase CFE of *Pvt1* inducible KO cells *in vitro.* Error bars represent S.D. **(G)** Immunoblots show inducible expression of *MYC* upon doxycycline (Dox) stimulation in engineered *Mettl14* KO cells. **(H)** The number of Krt10 (Keratin 10)-positive epidermal cells in skin grafts derived from *Mettl14* KO cells and *Mettl14* KO cells rescued with MYC expression was quantified and shown as bar graphs. n=4; P<0.01 (Student's t-test). Error bar represents S.D. **(I)** The number of suprabasal epidermal cells in skin grafts derived from *Mettl14* KO cells and *Mettl14* KO cells rescued with MYC expression was quantified and shown as box plots. n=14; P<0.01 (Student's t-test).

Appendix Figure S1

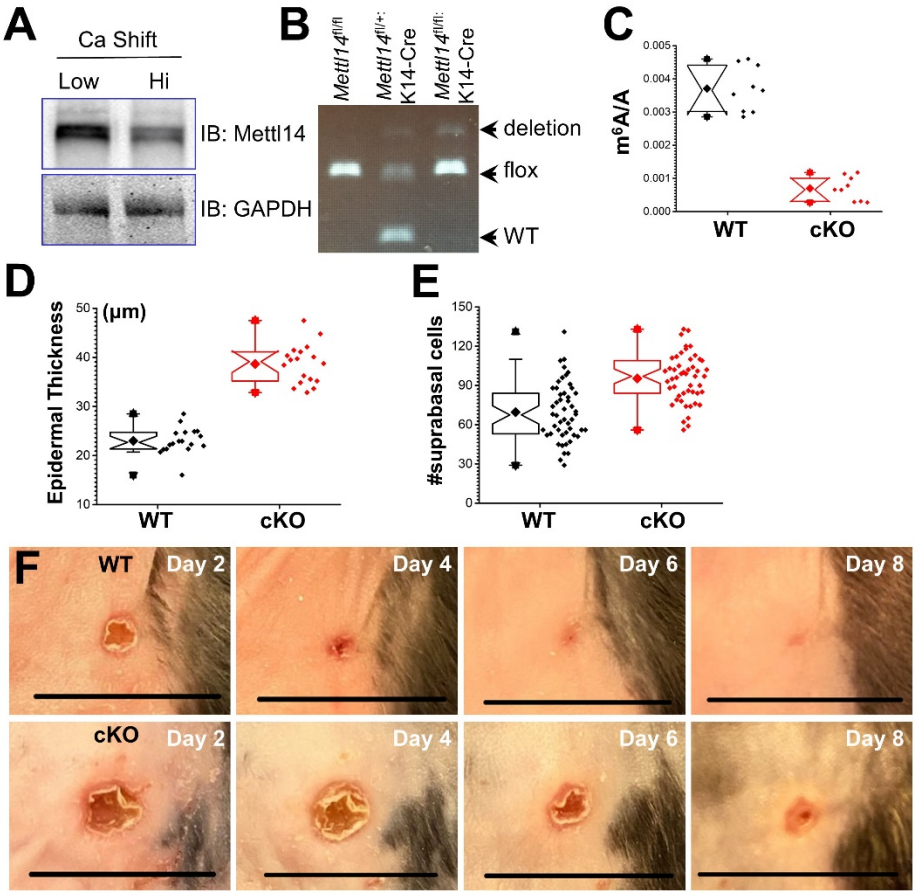

Appendix Figure S2

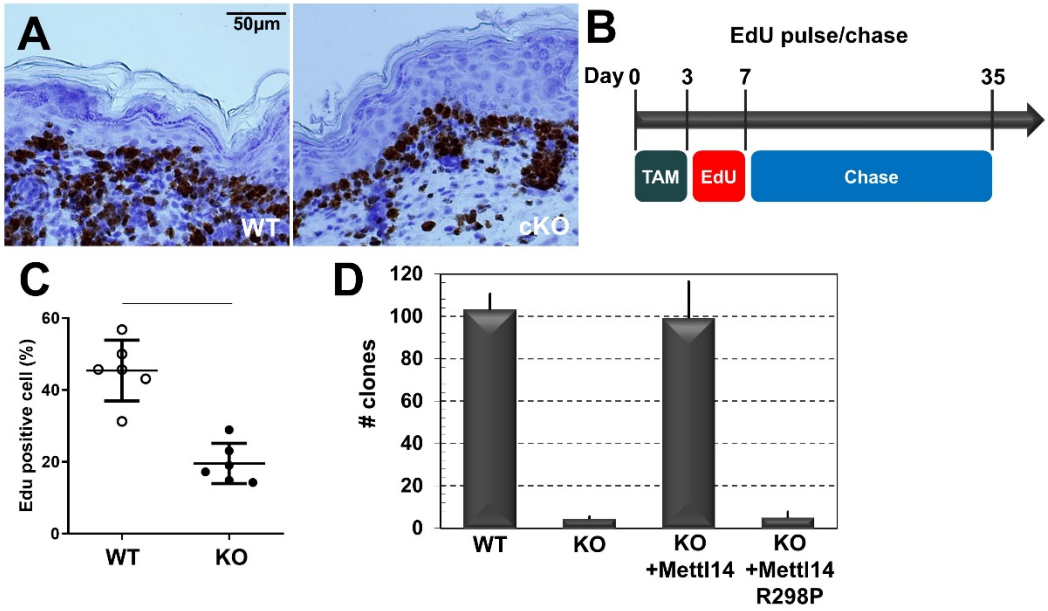

Appendix Figure S3

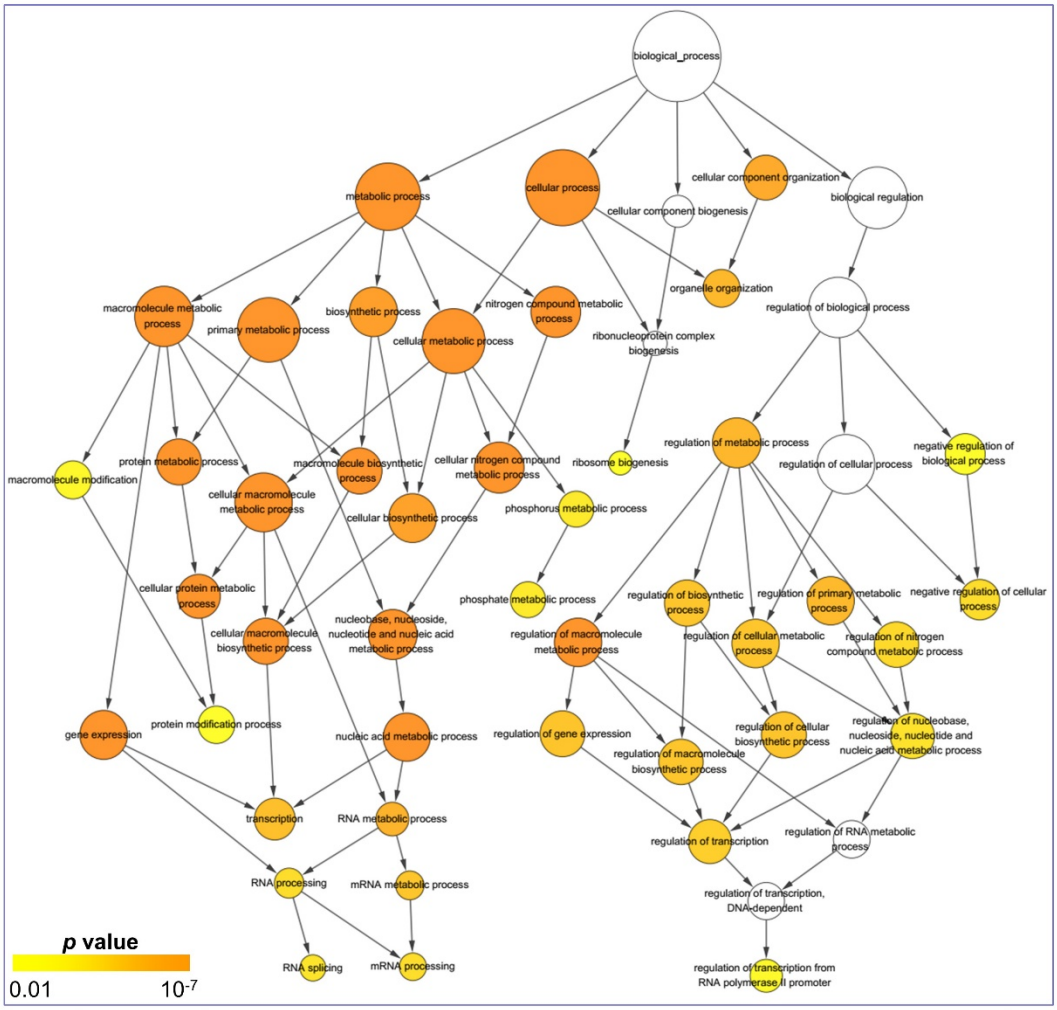

Appendix Figure S4

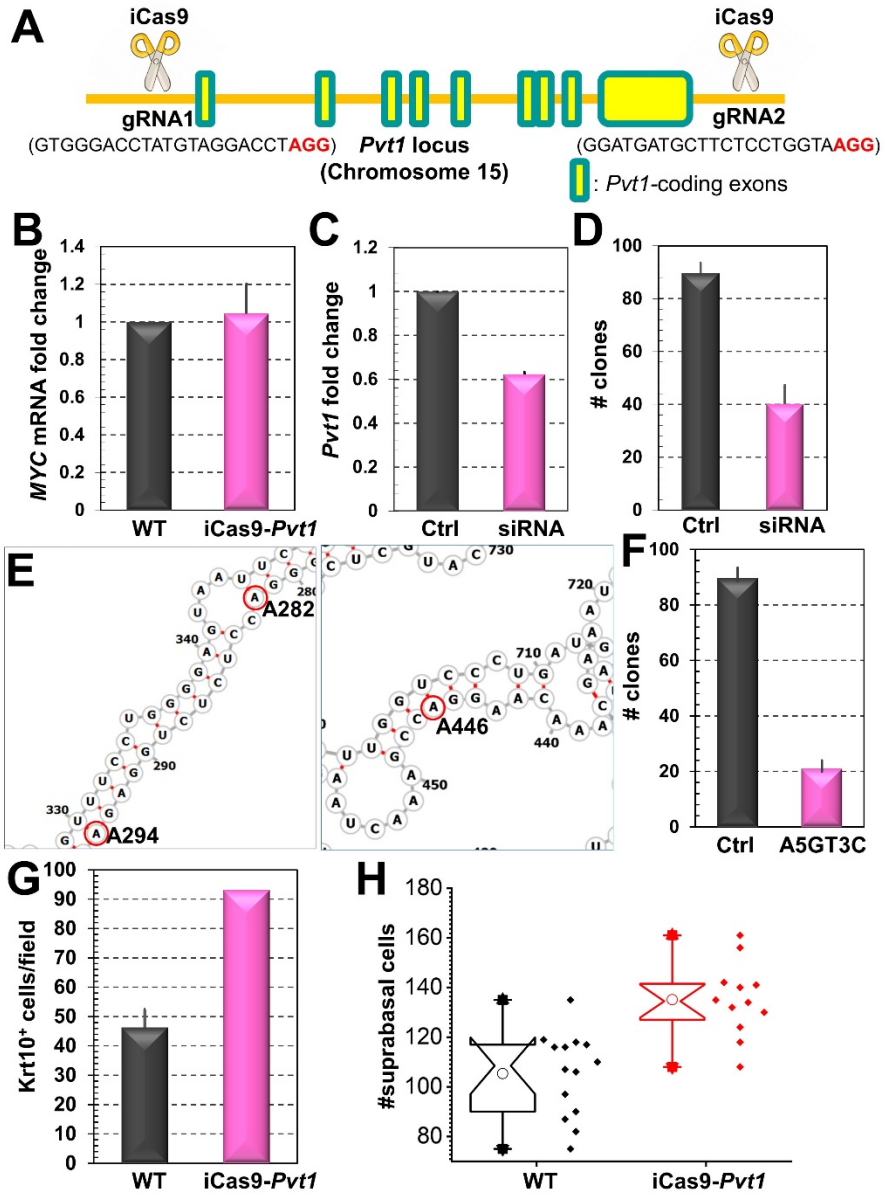
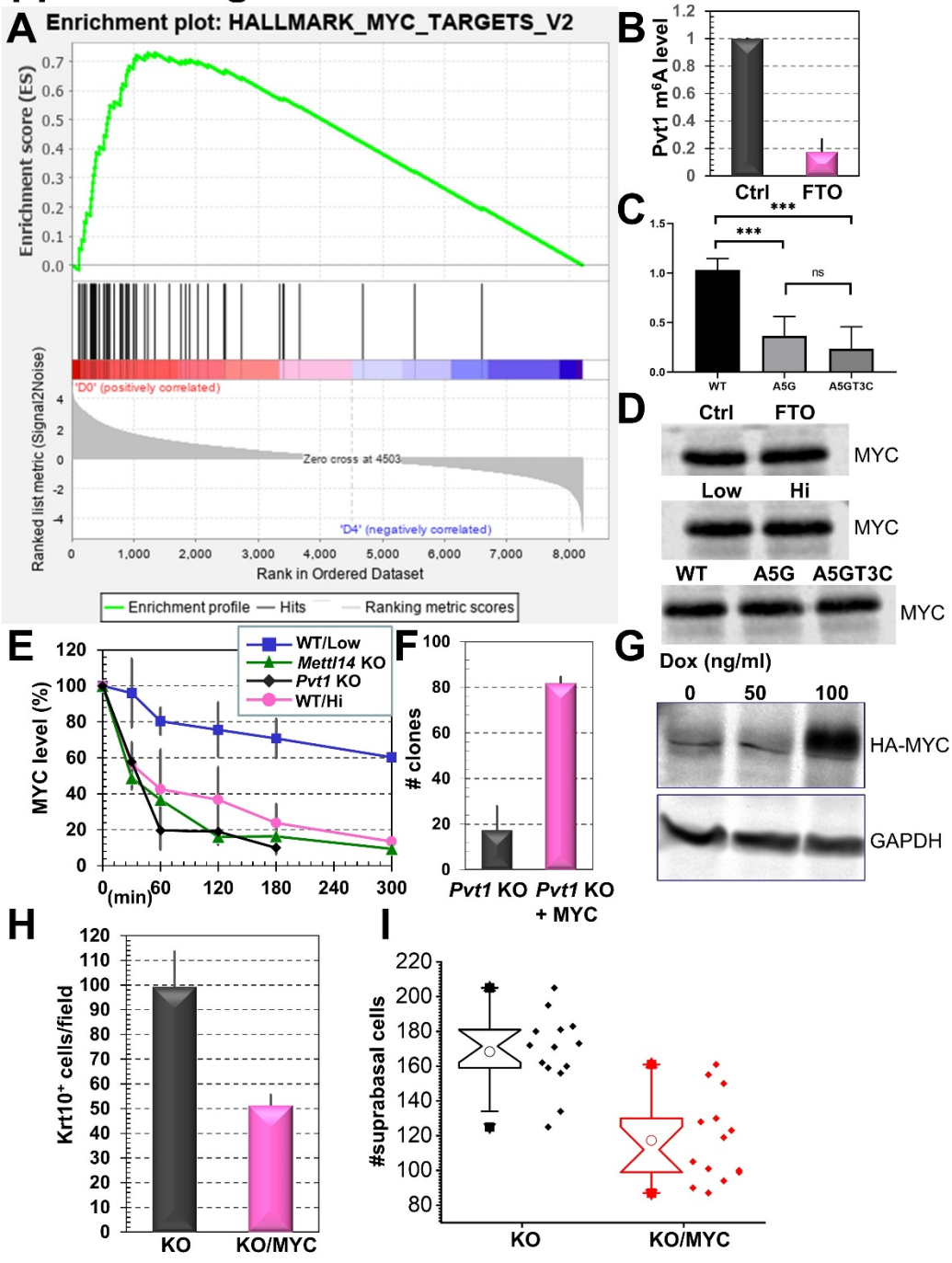
Appendix Figure S5